ACS APPLIED MATERIALS & INTERFACES

Research Article

www.acsami.org

Fast Diffusion of O_2 on Nitrogen-Doped Graphene to Enhance Oxygen Reduction and Its Application for High-Rate Zn−Air Batteries

Lei-Lei Tian,[†] Jie Yang,[†] Mou-Yi Weng,[†] Rui Tan,[†] Jia-Xin Zheng,*[,†] Hai-Biao Chen,*[,†] Quan-Chao Zhuang,[‡] Li-Ming Dai,[§] and Feng Pan*[,†]

[†]School of Advanced Materials, Shenzhen Graduate School, Peking University, Shenzhen 518055, China

[‡]School of Materials Science and Engineering, China University of Mining & Technology, Xuzhou 221116, China

[§]Department of Macromolecular Science and Engineering, Case Western Reserve University, 10900 Euclid Avenue, Cleveland, Ohio 44106, United States

Supporting Information

ABSTRACT: N-doped graphene (NDG) was investigated for oxygen reduction reaction (ORR) and used as air-electrode catalyst for Zn−air batteries. Electrochemical results revealed a slightly lower kinetic activity but a much larger rate capability for the NDG than commercial 20% Pt/C catalyst. The maximum power density for a Zn-air cell with NDG air cathode reached up to 218 mW cm^{-2}, which is nearly 1.5 times that of its counterpart with the Pt/C (155 mW cm^{-2}). The equivalent diffusion coefficient (D_E) of oxygen from electrolyte solution to the reactive sites of NDG was evaluated as about 1.5 times the liquid-phase diffusion coefficient (D_L) of oxygen within bulk electrolyte solution. Combined with experiments and ab initio calculations, this seems counterintuitive reverse ORR of NDG versus Pt/C can be rationalized by a spontaneous adsorption and fast solid-state diffusion of O_2 on ultralarge graphene surface of NDG to enhance effective ORR on *N*-doped-catalytic-centers and to achieve high-rate performance for Zn−air batteries.

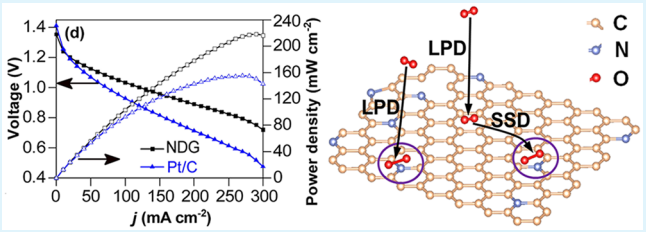

KEYWORDS: *oxygen reduction reaction, nitrogen-doped graphene, Zn−air battery, spillover, oxygen transport*

INTRODUCTION

Oxygen reduction reaction (ORR) is one of the most important processes for alkaline fuel cells and metal-air batteries.[1−3] To enhance effective ORR for high-power metal-air batteries, both high activity of the catalyst and fast diffusion of molecular oxygen (O_2) to catalytic-centers are synchronously required. N-doped graphene (NDG) has been intensively studied as an alternative ORR catalyst to noble-metal catalysts for dramatically reducing the cost, in which N-doping is the catalytic center to significantly decrease the energy barrier for intermediate steps of ORR to enhance the overall catalytic activity.[4−12] Despite much progress has been made in controlled synthesis of NDG catalysts,[2,4−14] the catalytic kinetic activities of the NDG were mostly evaluated under fast forced convective electrolyte with a well-defined oxygen transport by rotating disk electrode (RDE) measurements.[1,2,4−8,14,15] In practice, ORR reactions are carried out mostly in quiescent electrolyte(s), where the O_2 transport is different than that in fast forced convective electrolyte, it could be an important process of electrode reaction.[16−18] Generally, the O_2 transport of ORR could be mainly through two pathways: one is the concentration diffusion directly from electrolyte solution to the reactive sites, the other known as the spillover effect[17,18] is a multistep process involving the concentration diffusion of O_2 from electrolyte solution to the inactive regions, followed by a solid-surface diffusion to the reactive sites. Thus, the spillover effect involves the transport of active species adsorbed on one inactive surface site to another active surface site, which is an important process in the transport of active species, especially for the catalysts with heterogeneous surface regions and with dispersed active sites.[19,20]

N-doping could cause electron modulation to tune the surface properties and chemical (e.g., ORR) activities of graphene materials.[4−12,21] As catalyst, the active sites in NDG are mainly the N-doped structures, which may be separated by the mainly inactive undoped regions. So the NDG sheets could exhibit unique oxygen transport behaviors on graphene area, probably involving the spillover effect.[8,9] To the best of our knowledge, oxygen transport behaviors around the NDG catalysts and associated effects on ORR performance have rarely been studied. Herein, we report a reverse ORR of NDG versus Pt/C, in which NDG revealed a slightly lower kinetic activity in fast forced convective electrolyte but a much larger rate capability (nearly 1.5 times of power density) in quiescent electrolyte than that of commercial 20% Pt/C catalyst for Zn-

Received: November 27, 2016
Accepted: February 6, 2017
Published: February 6, 2017

DOI: 10.1021/acsami.6b15235
ACS Appl. Mater. Interfaces 2017, 9, 7125−7130

air batteries, and related mechanism investigated by experiments and ab initio calculations.

METHODS

Material Synthesis and Characterization. Dicyandiamide (DCDA, 99.5%) and monohydrate glucose (analytically pure) were used without further purification. In a typical synthesis, DCDA (48 g) and monohydrate glucose (2.4 g) were completely dissolved in deionized water under vigorous stirring, and then removed from the water. After drying, the obtained powder was enclosed in a tube furnace under argon atmosphere, and heated to 580 °C and preserved at this temperature for 4 h. Then, the temperature was increased up to 850 °C and maintained at this temperature for 6 h. NDG was obtained upon cooling down to room temperature.[22,23]

Transmission electron microscopy (TEM) images were recorded on a JEOL-2010 instrument at an acceleration voltage of 200 kV. The nitrogen doping structures and the surface chemistries of NDG were determined by X-ray photoelectron spectroscopy (XPS) (ESCALAB 250 Xi; Al anode). Raman measurements were carried out on a high-resolution, dispersive Raman spectrometer system (Horiba-Jobin Yvon LabRam HR) equipped with a visible laser excitation of 514 nm. Surface area and porosity were measured with standard nitrogen adsorption isotherms at 77 K by using an automated Micropore gas analyzer ASAP 2020 (Micromeritics Instruments).

Electrochemical Measurements. The ORR performance was carried out in an O_2-saturated 0.1 or 7 M KOH solution at 25 °C on a three-electrode-cell RDE system (Pine Inc.). The Pt-foil and Ag/AgCl electrode were used as auxiliary electrode and reference electrode, respectively. The catalyst ink for the working electrode was prepared by ultrasonic dispersion of NDG (2 mg) or equal weight of commercial 20% Pt/C catalyst (Alpha Aesar) and 5 wt % Nafion (200 μL) solution into 1.8 mL deionized water for 1 h. Then, the resultant ink (10 μL) was coated on the glassy carbon electrode (0.196 cm^2), with a catalyst loading of 51 $\mu g\ cm^{-2}$. The Zn-air cell was assembled by using Zn foil with thickness 500 μm (99%, Alfa Aesar) as counter electrode and 7 M KOH aqueous as electrolyte. The catalyst air electrode (2 cm^2) was prepared by uniformly coating another concentration of catalyst ink (2 mg mL^{-1}) on the commercial carbon paper (SGL Carbon Inc.) with a catalyst loading of 600 $\mu g\ cm^{-2}$. The detailed assembly and electrode reactions of the Zn-air cell please see SI section 4.

The electrochemical sweepings of RDE and static electrode were implemented on the Pine instrument system at predetermined scan rates and rotating speeds, while the chronoamperometry tests were carried out at −0.3 V vs Ag/AgCl in 0.1 M KOH solution at 1600 rpm. The galvanodynamic experiments were performed on the electrochemical workstation (PARSTAT 2273, Princeton Applied Research Inc.) with the current densities varied from 0 to 300 mA cm^{-2}. The galvanostatic discharge measurements were conducted with a battery testing system (Neware, Shenzhen). The reported specific capacities are all normalized to the weight of the consumed Zn.

Theoretical Calculations. The density functional theory (DFT) calculations were performed by using the Vienna Ab-initio Simulation Package (VASP)[24,25] using Perdew−Burke−Ernzerhof (PBE)[26] exchange-correlation functional with energy cutoff of 450 eV. During the geometry optimizations for oxygen molecule adsorption, the lattice constants were fixed. We set maximum residual force as 0.01 eV/Å and energy converge at 1×10^{-5} eV per atom. A vacuum buffer space of 20 Å was set for graphene slabs. A 7 × 7 × 1 Monkhorst−Pack was used for geometry optimization in a 5 × 5 supercell.[27] All the geometry optimization and energy were calculated by considering the solvation model supplemented in VASP 5.4 Package.[28,29] A DFT-D_2 semi-empirical dispersion-correction approach to correct the van der Waals (vdW) interactions and a dipole correction method were also tested in our calculations.[30]

RESULTS AND DISCUSSION

NDG sheets were synthesized by a bottom-up method according to the previously reported procedure.[22,23] Figure 1a shows typical TEM images for a NDG sheet, which displays a conspicuous wrinkled sheet in the scale of hundreds of nanometers. The energy filtered TEM results in (Figure S1) display a homogeneous distribution of C and N elements on NDG sheet, which certified nitrogen doped onto the carbon planes. The high resolution TEM (HRTEM) image (Figure 1b) discloses some disordered regions in the graphene layer, in consistent with the Raman results (Figure S2a), these regions are mainly caused by N-doping. The N-doped structures were confirmed by the XPS results. The sharp C 1s peak at around 284.6 eV (Figure S2d) is assigned to the sp^2-hybridized graphene framework, and the other peaks at higher binding energies are attributable to the oxygen- and/or nitrogen-containing groups attached to the aromatic ring of graphene.[22,23,31,32] The high-resolution O 1s XPS spectrum (Figure S2e) could be deconvoluted into 3 main components with the binding energies of 531.5, 532.6, and 533.8 eV, corresponding to the O−C, O═C, and O−C═O bonds, respectively.[33] The N content in NDG was determined to be 13.1 at% by the XPS survey spectrum (Figure S2c). According to the curve-fitted high-resolution XPS N 1s spectrum (Figure 1c), we can conclude that N-dopants in the NDG are mainly in three forms: pyridinic N (398.2 eV), pyrrolic N (400.2 eV), and graphitic N (400.9 eV).[22,23,31,32]

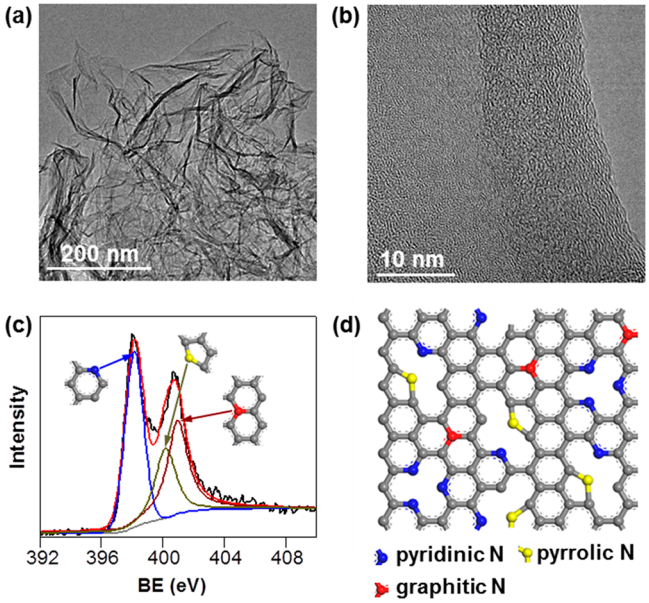

Figure 1. Representative (a) TEM, (b) HRTEM images, (c) XPS N 1s spectra, and (d) schematic nitrogen structure models of NDG.

The ORR kinetic activity of the NDG was investigated by RDE measurements in O_2-saturated 0.1 M KOH solution at 1600 rpm. For comparison, the commercial 20 wt % Pt/C catalyst was also tested under the same condition. The linear voltammetic sweep (LSV) curves are given in Figure 2a, which shows onset and half-wave potentials of about −0.06 and −0.18 V (vs Ag/AgCl), respectively; the NDG electrode, which are slightly more negative than those of Pt/C (0.03 and −0.12 V, respectively), indicating a more sluggish catalytic activity for the NDG than that of the Pt/C. The durability of the catalysts was evaluated by the chronoamperometric testing at −0.3 V (vs Ag/AgCl), and the NDG electrode displayed 18% decay of current density over 35 000 s continuous testing, which is much lower than that of the Pt/C electrode (34%) (Figure 2b). The observed superior stability for NDG with respect to Pt/C is

DOI: 10.1021/acsami.6b15235
ACS Appl. Mater. Interfaces 2017, 9, 7125−7130

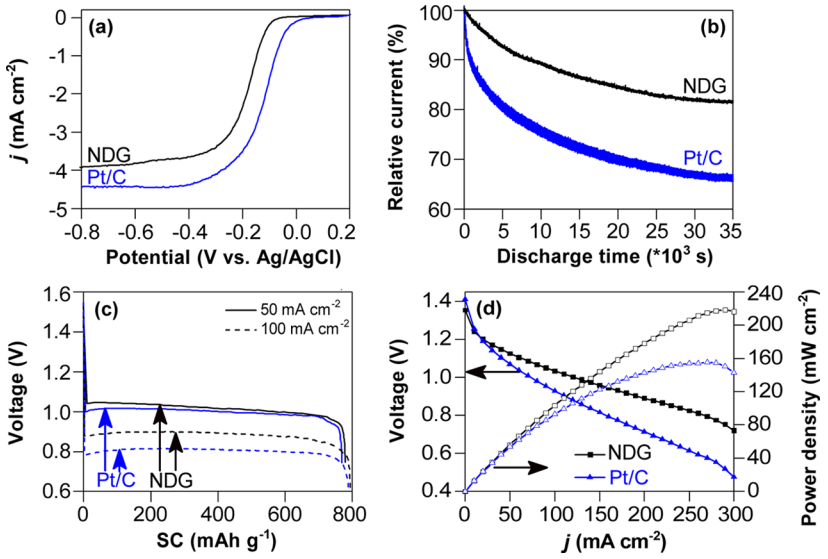

Figure 2. ORR catalytic activity and Zn-air battery performance of NDG (black curves) and commercial Pt/C (blue curves). (a) RDE voltammograms with sweep rate of 10 mV s^{-1} and (b) the relative current−time responses at −0.3 V vs Ag/AgCl in 0.1 M KOH solution at 1600 rpm. (c) Discharge curves and (d) polarization curves and the corresponding power density plots of NDG and Pt/C electrodes in 7 M KOH solution with fresh Zn anode. The current densities (j) are normalized to the geometric area of the working electrodes.

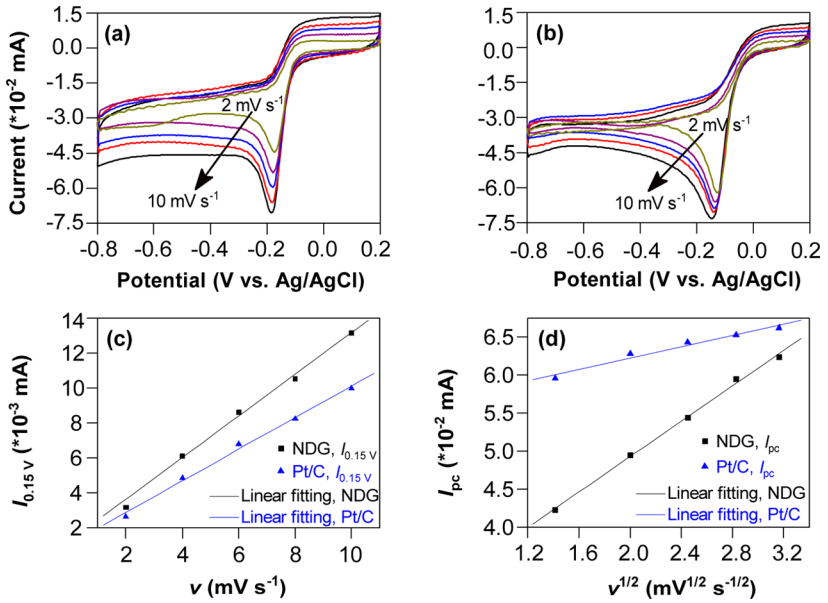

Figure 3. Cyclic voltammograms of (a) NDG and (b) commercial Pt/C in static O_2 saturated 0.1 M KOH solution at the scan rate (v) of 2, 4, 6, 8, and 10 mV s^{-1}; plots of (c) anodic current at 0.15 V ($I_{0.15\ V}$) vs scan rate (v) and (d) cathodic peak current (I_{pc}) vs the root of scan rate ($v^{1/2}$).

consistent with almost all of the previous reports on carbon-based metal-free ORR catalysts.[34,35] Given that more concentrated KOH solutions are generally used in Zn-air cells,[36] we also carried out the LSV measurements in O_2-saturated 7 M KOH solution. Similar catalytic behaviors were observed even the highly concentrated KOH solution (Figure S5a), though the relatively low oxygen concentration in and high viscosity of the electrolyte solution could have a detrimental effect on the ORR performance.[32,37,38]

We also fabricated Zn-air cells with the NDG or Pt/C as air cathode catalyst, 7 M KOH solution was used as electrolyte. Interestingly, at the galvanostatic discharging current densities of 50 and 100 mA cm^{-2} (Figure 2c), the cells with the NDG air cathode achieved specific capacities (normalized to the weight of the consumed zinc) of 778 and 793 mAh g^{-1}, respectively, which are slightly higher than that of the Pt/C catalyst (769 and 788 mAh g^{-1}, respectively), and much higher than the reported values for zinc-air batteries (Table S1).[10−12,21,39] Thereafter, we replaced the consumed Zn anode with another fresh one, and assembled the cell with the air cathode which we used once already. The new cell could discharge for another 2 h with a stable voltage at the current density of 50 mA cm^{-2}, and delivered a specific capacity of 780 mAh g^{-1} (Figure S5b). Therefore, the failure of the cells was mainly due to the accumulation of unfavorable byproducts on Zn anode these may hinder the further electrode reactions.[38] It is worthwhile to notice that the cells with the NDG air cathode delivered higher working voltages and power densities than those of their counterparts with the Pt/C at the same current density, especially at high rate discharging (Figure 2d). The maximum

DOI: 10.1021/acsami.6b15235
ACS Appl. Mater. Interfaces 2017, 9, 7125−7130

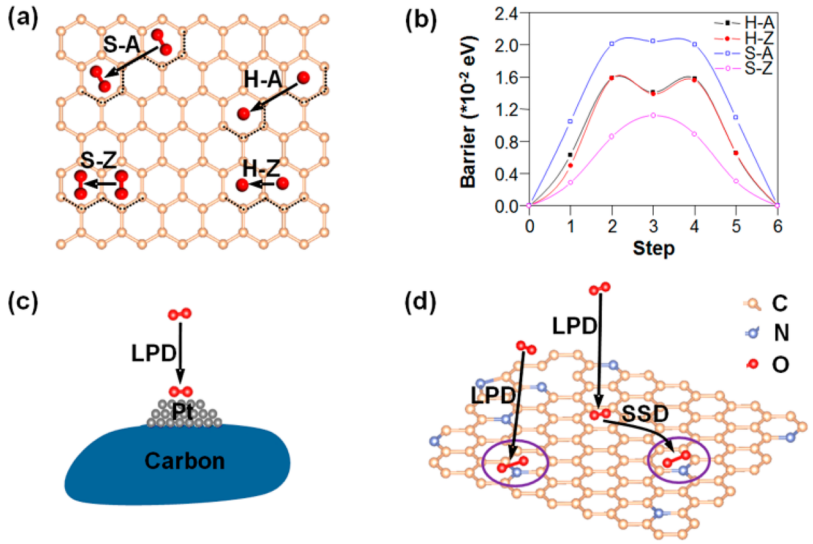

Figure 4. (a) Four kinds of molecule oxygen diffusion modes on a graphene layer and (b) the corresponding diffusion energy barriers obtained by theoretical calculations. Schematic illustrations for the molecular oxygen transport to the reactive sites of (c) Pt/C and (d) NDG. H-A, H-Z, S-A, and S-Z denote head-on-armchair, head-on-zigzag, side-on-armchair, and side-on-zigzag, respectively; purple circle marked regions in panel d denote the ORR reactive sites of NDG.

power density for the cell with the NDG air cathode is 218 mW cm^{-2}, nearly 1.5 times which of the Pt/C air cathode (155 mW cm^{-2}). Also, the pristine graphene exhibited a much more sluggish ORR catalytic activity and lower cell powder density (76.6 mW cm^{-2}, see SI section 9). These results illustrated that the NDG could achieve a superior electrochemical catalytic performance in practical Zn-air batteries with respect to the commercial Pt/C catalyst, though a slight lower kinetic activity was observed by the RDE measurements.

To understand these seemingly contradictory results, we further investigated the electrode processes of the catalysts by the cyclic voltammetry (CV) with various scan rates. The CV curves within the ORR inactive potential range (0−0.2 V vs Ag/AgCl) appeared typical quasi-rectangular (Figure 3a-b, Figure S6), indicating the capacitive processes on the catalyst electrodes, as confirmed by the linear $I_{0.15V}$−ν plots in Figure 3c.[2,32] Thereafter, the catalytic ORR occurred within the more negative potential range, which is a diffusion limited process as confirmed by the linear I_{pc}−$\nu^{1/2}$ plots in Figure 3d. During the diffusion limited reaction, the oxygen transport behaviors could be characterized by the equivalent diffusion coefficient (D_E) that is deduced from the equation of diffusion limiting current (I_D) to scan rate (ν), as in eq 1[15,40]

$$I_D = 0.4958nFAC^*D_E^{1/2}(n\alpha F/RT)^{1/2}\nu^{1/2} \quad (1)$$

The electrochemical active area (A) of the catalyst electrode is proportional to the capacitive current,[15,41] where the A ratio of NDG to Pt/C ($A_{NDG}/A_{Pt/C}$) was roughly evaluated from the slopes of $I_{0.15V}$−ν plots to be 1.35. Accordingly, the D_E ratio (NDG to Pt/C) can be determined from the slopes of the I_D−$\nu^{1/2}$ plots to be 1.5. According to the Levich plots of Pt/C (see SI section 8), we speculated that the oxygen transport on Pt/C is nearly by the direct liquid-phase diffusion of molecular oxygen with a diffusion coefficient (D_L) of 1.9×10^{-5} cm^2 s^{-1}.[37] Therefore, the D_E on NDG can be calculated to be 2.85×10^{-5} cm^2 s^{-1}. The enhanced oxygen diffusion for NDG is probably resulted mainly from the large area of graphene to supply the solid-surface diffusion along with the NDG layer,[42−44] and hence the improved overall oxygen transport to the reactive sites.

The experimental findings were confirmed and further clarified by DFT calculations, during which the solvation model[28] combined with nudged elastic band (NEB) method[45] were used. To investigate the adsorption of O_2 on NDG, we constructed and studied 13 possible configurations (see SI section 10). The adsorption energies around −0.27 eV, indicated that O_2 can be spontaneously absorbed on undoped graphene regions of NDG layer, and the equilibrium distance around 2.9 Å of O_2 on undoped graphene indicated a weak chemisorption. Among the configurations, all the side-on adsorptions showed larger adsorption energies than head-on adsorptions. Given the situation of negative energy on all configurations and average 0.05 eV difference between the energies of side-on and head-on adsorptions, we speculated that O_2 can be absorbed on undoped graphene layer by any configuration but the side-on types have more probability. Compared with that on pristine graphene, O_2 adsorption on graphitic N site exhibited a much stronger adsorption with adsorption energy of −0.64 eV and a shorter equilibrium distance of 2.77 Å. In pyridinic and pyrrolic N doped graphene, it turned out that the absorption also become much stronger than the adsorptions on pristine graphene (Figure S9 and Table S2). These results indicate that graphitic, pyridinic, and pyrrolic N sites are more active than the undoped sites. Also, our study of the diffusion of molecular oxygen toward N site has shown a very tiny energy barrier and a significant trend to diffusion (Figure S11a). For studying the diffusivity, we considered 4 diffusion pathways of molecular oxygen: side-on-armchair, side-on-zigzag, head-on-armchair, and head-on-zigzag diffusion (Figure 4a). We did all these NEB calculations on a graphene layer for convenience, as pervious calculation test has proved the diffusion coefficient calculated on pristine graphene and NDG are similar (Figure S11b). Among these pathways, head-on-zigzag diffusion showed the lowest barrier of 0.015 eV (Figure 4b), indicating the most liable diffusion path. While other paths have higher barriers, the energies are close to that of head-on zigzag diffusion, thus the other three paths are also

DOI: 10.1021/acsami.6b15235
ACS Appl. Mater. Interfaces 2017, 9, 7125−7130

possible for O_2 diffusion. The solid-surface diffusion coefficient (D_S) can be evaluated by the eq 2[46,47]

$$D_S = a^2 \nu^* \exp(-E_{act}/k_B T) \quad (2)$$

where ν^*, E_{act}, and a are the attempt frequency, the activation barrier and the distance of hop path, respectively. Here a is 4.26 Å in armchair paths and 2.46 Å in zigzag paths, ν^* is 10^{13} Hz and generally in the range of phonon frequency,[47] and T is 300 K. Accordingly, the D_S can be estimated as $\sim 10^{-2}$ cm^2 s^{-1}. Comparing with the liquid-phase diffusion ($D_L = 1.9 \times 10^{-5}$ cm^2 s^{-1}, vide supra) of molecular oxygen in electrolyte solution, the solid-surface diffusion of O_2 along with the graphene layer is much faster (about 3 orders), which could be attributed to the weak chemisorption of oxygen on graphene that decreased the interaction between oxygen and water molecules.

On the basis of the above analyses, a schematic drawing (Figure 4c and d) is given as a working model to illustrate the oxygen transport. The ORR reactive sites on the graphene layer were mostly separated by the inactive (undoped graphene) regions. During ORR, the O_2 molecules could be transported to the reactive sites through two paths, one is the liquid-phase-diffusion (denoted LPD) of O_2 molecules direct from the bulk electrolyte solution to the reactive sites; another is the LPD of O_2 molecules from the bulk electrolyte solution to the inactive graphene regions of the NDG layer, followed by migration to the reactive sites by solid-surface diffusion (denoted SSD) along with the graphene layer - that is a kind of typical spillover effect. The superimposed two paths can lead to an increased overall diffusion of O_2 transport to the reactive sites of NDG, particularly when the high diffusion rate is ensured for the SSD. This was confirmed by the electrochemical results and theory calculations, which is also indicative of the effectiveness of O_2 SSD along with the graphene layer.

CONCLUSIONS

In summary, NDG was investigated for ORR and used as air-electrode catalyst for Zn−air batteries. Electrochemical results revealed a slightly lower kinetic activity but a much larger rate capability for the NDG than commercial 20% Pt/C catalyst. The maximum power density for a Zn-air cell with NDG air cathode reached up to 218 mW cm^{-2}, which is nearly 1.5 times that of its counterpart with the Pt/C (155 mW cm^{-2}). The equivalent diffusion coefficient of O_2 to the reactive sites of NDG was evaluated as about 1.5 times the liquid-phase diffusion coefficient of oxygen within bulk electrolyte solution. Combined with experiments and ab initio calculations, this reverse ORR of NDG vs Pt/C can be rationalized by a spontaneous absorption and fast solid-surface diffusion of O_2 on NDG to enhance ORR on N-doped-catalytic-centers and to achieve high-rate performance for Zn-Air batteries. This work revealed the spontaneous adsorption and the possible fast diffusion of O_2 along graphene layers and spillover effect for N-doped graphene, and provides a new way for enhancing the electrochemical performance for NDG catalysts for ORR in energy conversion and storage devices (e.g., metal−air batteries, fuel cells) of practical significance and beyond.

ASSOCIATED CONTENT

Supporting Information

The Supporting Information is available free of charge on the ACS Publications website at DOI: 10.1021/acsami.6b15235.

Absorption and diffusion models of molecular oxygen on NDG, supplementary characterization results and discussions (PDF)

AUTHOR INFORMATION

Corresponding Authors

*E-mail: panfeng@pkusz.edu.cn.
*E-mail: chenhb@pkusz.edu.cn.
*E-mail: zhengjx@pkusz.edu.cn.

ORCID

Feng Pan: 0000-0002-8216-1339

Author Contributions

L.L.T., J.Y. and M.Y.W. contributed equally to this work. L.L.T. and J.Y. conceived, designed, and carried out the experiments and analyzed the data. M.Y.W. preformed the theoretical calculations. All authors discussed the results and commented on the manuscript.

Notes

The authors declare no competing financial interest.

ACKNOWLEDGMENTS

The authors acknowledge financial support from the Fund from the Guangdong Innovation Team Project (No. 2013N080) and the Shenzhen Science and Technology Research Grant (No. JCYJ20150629144526408).

REFERENCES

(1) Ge, X. M.; Sumboja, A.; Wuu, D.; An, T.; Li, B.; Goh, F. W. T.; Hor, T. S. A.; Zong, Y.; Liu, Z. L. Oxygen Reduction In Alkaline Media: From Mechanisms to Recent Advances of Catalysts. *ACS Catal.* **2015**, *5*, 4643−4667.

(2) Jiang, S.; Zhu, C. Z.; Dong, S. J. Cobalt and Nitrogen-Cofunctionalized Graphene as A Durable Non-Precious Metal Catalyst with Enhanced ORR Activity. *J. Mater. Chem. A* **2013**, *1*, 3593−3599.

(3) Winter, M.; Brodd, R. J. What Are Batteries, Fuel Cells, and Supercapacitors? *Chem. Rev.* **2004**, *104*, 4245−4270.

(4) Sharifi, T.; Hu, G.; Jia, X. E.; Wagberg, T. Formation of Active Sites for Oxygen Reduction Reactions by Transformation of Nitrogen Functionalities in Nitrogen-Doped Carbon Nanotubes. *ACS Nano* **2012**, *6*, 8904−8912.

(5) Lai, L. F.; Potts, J. R.; Zhan, D.; Wang, L.; Poh, C. K.; Tang, C. H.; Gong, H.; Shen, Z. X.; Lin, J.; Ruoff, R. S. Exploration of The Active Center Structure of Nitrogen-Doped Graphene-Based Catalysts for Oxygen Reduction Reaction. *Energy Environ. Sci.* **2012**, *5*, 7936−7942.

(6) Gong, Y. J.; Fei, H. L.; Zou, X. L.; Zhou, W.; Yang, S. B.; Ye, G. L.; Liu, Z.; Peng, Z. W.; Lou, J.; Vajtai, R.; Yakobson, B. I.; Tour, J. M.; Ajayan, P. M. Boron- and Nitrogen-Substituted Graphene Nanoribbons as Efficient Catalysts for Oxygen Reduction Reaction. *Chem. Mater.* **2015**, *27*, 1181−1186.

(7) Lin, Z. Y.; Waller, G.; Liu, Y.; Liu, M. L.; Wong, C. P. Facile Synthesis of Nitrogen-Doped Graphene Via Pyrolysis of Graphene Oxide and Urea, and Its Electrocatalytic Activity Toward The Oxygen-Reduction Reaction. *Adv. Energy Mater.* **2012**, *2*, 884−888.

(8) Zhang, Y. W.; Ge, J.; Wang, L.; Wang, D. H.; Ding, F.; Tao, X. M.; Chen, W. Manageable N-Doped Graphene for High Performance Oxygen Reduction Reaction. *Sci. Rep.* **2013**, *3*, 2771.

(9) Yu, L.; Pan, X. L.; Cao, X. M.; Hu, P.; Bao, X. H. Oxygen Reduction Reaction Mechanism on Nitrogen-Doped Graphene: A Density Functional Theory Study. *J. Catal.* **2011**, *282*, 183−190.

(10) Nam, G.; Park, J.; Sun, T. K.; Shin, D. B.; Park, N.; Kim, Y.; Lee, J.-S.; Cho, J. Metal-Free Ketjenblack Incorporated Nitrogen-Doped Carbon Sheets Derived from Gelatin as Oxygen Reduction Catalysts. *Nano Lett.* **2014**, *14*, 1870−1876.

DOI: 10.1021/acsami.6b15235
ACS Appl. Mater. Interfaces 2017, 9, 7125−7130

(11) Kashyap, V.; Singh, S. K.; Kurungot, S. Cobalt Ferrite Bearing Nitrogen-Doped Reduced Graphene Oxide Layers Spatially Separated with Microporous Carbon as Efficient Oxygen Reduction Electrocatalyst. *ACS Appl. Mater. Interfaces* **2016**, *8*, 20730−20740.
(12) Wang, M.; Fang, Z.; Zhang, K.; Fang, J.; Qin, F.; Zhang, Z.; Li, J.; Liu, Y.; Lai, Y. Synergistically Enhanced Activity of Graphene Quantum Dots/Graphene Hydrogel Composites: A Novel All-Carbon Hybrid Electrocatalyst for Metal/Air Batteries. *Nanoscale* **2016**, *8*, 11398−11402.
(13) Gong, K. P.; Du, F.; Xia, Z. H.; Durstock, M.; Dai, L. M. Nitrogen-Doped Carbon Nanotube Arrays with High Electrocatalytic Activity for Oxygen Reduction. *Science* **2009**, *323*, 760−764.
(14) Li, Y. G.; Zhou, W.; Wang, H. L.; Xie, L. M.; Liang, Y. Y.; Wei, F.; Idrobo, J. C.; Pennycook, S. J.; Dai, H. J. An Oxygen Reduction Electrocatalyst Based on Carbon Nanotube-Graphene Complexes. *Nat. Nanotechnol.* **2012**, *7*, 394−400.
(15) Bard, A. J.; Faulkner, L. R. *Electrochemical Methods: Fundamentals and Applications*; John Wiley & Sons, Inc., 2000; pp 331−338.
(16) Chaparro, A. M.; Martin, A. J.; Daza, L. Theoretical Analysis of the Limiting Diffusion Current at a 'Particulate Rotating Disk Electrode'. *ECS Trans.* **2009**, *25*, 125−133.
(17) Chaparro, A. M. Study of Spillover Effects with The Rotating Disk Electrode. *Electrochim. Acta* **2011**, *58*, 691−698.
(18) Chaparro, A. M. Analysis of the Steady State and Transient Currents for a Rotating Disk Electrode under Surface Diffusion Limitation. *J. Electrochem. Soc.* **2014**, *161*, E3078−E3085.
(19) Khoobiar, S. Particle to Particle Migration of Hydrogen Atoms on Platinum-Alumina Catalysts from Particle to Neighboring Particles. *J. Phys. Chem.* **1964**, *68*, 411−412.
(20) Conner, W. C.; Falconer, J. L. Spillover in Heterogeneous Catalysis. *Chem. Rev.* **1995**, *95*, 759−788.
(21) Park, G. S.; Lee, J. S.; Kim, S. T.; Park, S.; Cho, J. Porous Nitrogen Doped Carbon Fiber with Churros Morphology Derived from Electrospun Bicomponent Polymer as Highly Efficient Electrocatalyst for Zn-Air Batteries. *J. Power Sources* **2013**, *243*, 267−273.
(22) Tian, L. L.; Wei, X. Y.; Zhuang, Q. C.; Jiang, C. H.; Wu, C.; Ma, G. Y.; Zhao, X.; Zong, Z. M.; Sun, S. G. Bottom-Up Synthesis of Nitrogen-Doped Graphene Sheets for Ultrafast Lithium Storage. *Nanoscale* **2014**, *6*, 6075−6083.
(23) Tian, L. L.; Li, S. B.; Zhang, M. J.; Li, S. K.; Lin, L. P.; Zheng, J. X.; Zhuang, Q. C.; Amine, K.; Pan, F. Cascading Boost Effect on the Capacity of Nitrogen-Doped Graphene Sheets for Li-and Na-Ion Batteries. *ACS Appl. Mater. Interfaces* **2016**, *8*, 26722−26729.
(24) Kresse, G.; Furthmuller, J. Efficient Iterative Schemes for Ab Initio Total-Energy Calculations Using A Plane-Wave Basis Set. *Phys. Rev. B: Condens. Matter Mater. Phys.* **1996**, *54*, 11169−11186.
(25) Kresse, G.; Furthmuller, J. Efficiency of Ab-Initio Total Energy Calculations for Metals and Semiconductors Using A Plane-Wave Basis Set. *Comput. Mater. Sci.* **1996**, *6*, 15−50.
(26) Perdew, J. P.; Burke, K.; Ernzerhof, M. Generalized Gradient Approximation Made Simple. *Phys. Rev. Lett.* **1996**, *77*, 3865−3868.
(27) Monkhorst, H. J.; Pack, J. D. Special Points for Brillouin-Zone Integrations. *Phys. Rev. B* **1976**, *13*, 5188−5192.
(28) Mathew, K.; Sundararaman, R.; Letchworth-Weaver, K.; Arias, T. A.; Hennig, R. G. Implicit Solvation Model for Density-Functional Study of Nanocrystal Surfaces and Reaction Pathways. *J. Chem. Phys.* **2014**, *140*, 084106.
(29) Sakong, S.; Naderian, M.; Mathew, K.; Hennig, R. G.; Gross, A. Density Functional Theory Study of The Electrochemical Interface Between A Pt Electrode and An Aqueous Electrolyte Using An Implicit Solvent Method. *J. Chem. Phys.* **2015**, *142*, 234107.
(30) Grimme, S. Semiempirical GGA-Type Density Functional Constructed with A Long-Range Dispersion Correction. *J. Comput. Chem.* **2006**, *27*, 1787−1799.
(31) Tian, L.; Zhuang, Q.; Li, J.; Wu, C.; Shi, Y.; Sun, S. The Production of Self-Assembled Fe_2O_3-Graphene Hybrid Materials by A Hydrothermal Process for Improved Li-Cycling. *Electrochim. Acta* **2012**, *65*, 153−158.
(32) Li, H.; Liu, H.; Jong, Z.; Qu, W.; Geng, D. S.; Sun, X. L.; Wang, H. J. Nitrogen-Doped Carbon Nanotubes with High Activity for Oxygen Reduction in Alkaline Media. *Int. J. Hydrogen Energy* **2011**, *36*, 2258−2265.
(33) Shao, Y.; Zhang, S.; Engelhard, M. H.; Li, G.; Shao, G.; Wang, Y.; Liu, J.; Aksay, I. A.; Lin, Y. Nitrogen-Doped Graphene and Its Electrochemical Applications. *J. Mater. Chem.* **2010**, *20*, 7491−7496.
(34) Dai, L. M.; Xue, Y. H.; Qu, L. T.; Choi, H. J.; Baek, J. B. Metal-Free Catalysts for Oxygen Reduction Reaction. *Chem. Rev.* **2015**, *115*, 4823−4892.
(35) Shui, J.; Wang, M.; Du, F.; Dai, L. M. N-Doped Carbon Nanomaterials Are Durable Catalysts for Oxygen Reduction Reaction in Acidic Fuel Cells. *Sci. Adv.* **2015**, *1*, e1400129.
(36) Xu, M.; Ivey, D. G.; Xie, Z.; Qu, W. Rechargeable Zn-Air Batteries: Progress in Electrolyte Development and Cell Configuration Advancement. *J. Power Sources* **2015**, *283*, 358−371.
(37) Davis, R. E.; Horvath, G. L.; Tobias, C. W. The Solubility and Diffusion Coefficient of Oxygen in Potassium Hydroxide Solutions. *Electrochim. Acta* **1967**, *12*, 287−297.
(38) Lee, J. S.; Park, G. S.; Lee, H. I.; Kim, S. T.; Cao, R. G.; Liu, M. L.; Cho, J. Ketjenblack Carbon Supported Amorphous Manganese Oxides Nanowires as Highly Efficient Electrocatalyst for Oxygen Reduction Reaction in Alkaline Solutions. *Nano Lett.* **2011**, *11*, 5362−5366.
(39) Zhang, X.; Liu, R.; Zang, Y.; Liu, G.; Wang, G.; Zhang, Y.; Zhang, H.; Zhao, H. Co/CoO Nanoparticles Immobilized on Co-N-Doped Carbon as Trifunctional Electrocatalysts for Oxygen Reduction, Oxygen Evolution and Hydrogen Evolution Reactions. *Chem. Commun.* **2016**, *52*, 5946−5949.
(40) Tian, L. L.; Zhang, M. J.; Wu, C.; Wei, Y.; Zheng, J. X.; Lin, L. P.; Lu, J.; Amine, K.; Zhuang, Q. C.; Pan, F. γ-Fe_2O_3 Nanocrystalline Microspheres with Hybrid Behavior of Battery- Supercapacitor for Superior Lithium Storage. *ACS Appl. Mater. Interfaces* **2015**, *7*, 26284−26290.
(41) Ma, T. Y.; Dai, S.; Jaroniec, M.; Qiao, S. Z. Metal-Organic Framework Derived Hybrid Co_3O_4-Carbon Porous Nanowire Arrays as Reversible Oxygen Evolution Electrodes. *J. Am. Chem. Soc.* **2014**, *136*, 13925−13931.
(42) Frank, B.; Blume, R.; Rinaldi, A.; Trunschke, A.; Schlogl, R. Oxygen Insertion Catalysis by sp2 Carbon. *Angew. Chem., Int. Ed.* **2011**, *50*, 10226−10230.
(43) Mehmood, F.; Pachter, R.; Lu, W. J.; Boeckl, J. J. Adsorption and Diffusion of Oxygen on Single-Layer Graphene with Topological Defects. *J. Phys. Chem. C* **2013**, *117*, 10366−10374.
(44) Radovic, L. R.; Suarez, A.; Vallejos-Burgos, F.; Sofo, J. O. Oxygen Migration on The Graphene Surface. 2. Thermochemistry of Basal-Plane Diffusion (Hopping). *Carbon* **2011**, *49*, 4226−4238.
(45) Henkelman, G.; Uberuaga, B. P.; Jonsson, H. A Climbing Image Nudged Elastic Band Method for Finding Saddle Points and Minimum Energy Paths. *J. Chem. Phys.* **2000**, *113*, 9901−9904.
(46) Vineyard, G. H. Frequency Factors and Isotope Effects in Solid State Rate Processes. *J. Phys. Chem. Solids* **1957**, *3*, 121−127.
(47) Morgan, D.; Van der Ven, A.; Ceder, G. Li Conductivity in Li_xMPO_4 (M= Mn, Fe, Co, Ni) Olivine Materials. *Electrochem. Solid-State Lett.* **2004**, *7*, A30−A32.

DOI: 10.1021/acsami.6b15235
ACS Appl. Mater. Interfaces 2017, 9, 7125−7130